Title: Femtosecond laser ablation of aluminum in vacuum and air at high laser intensity

Author: Xin Zhao Yung C. Shin

PII: S0169-4332(13)01136-7
DOI: http://dx.doi.org/doi:10.1016/j.apsusc.2013.06.037
Reference: APSUSC 25840

To appear in: *APSUSC*

Received date: 18-2-2013
Revised date: 17-5-2013
Accepted date: 6-6-2013

Please cite this article as: X. Zhao, Y.C. Shin, Femtosecond laser ablation of aluminum in vacuum and air at high laser intensity, *Applied Surface Science* (2013), http://dx.doi.org/10.1016/j.apsusc.2013.06.037

Femtosecond laser ablation of aluminum in vacuum and air at high laser intensity

Xin Zhao and Yung C. Shin

Center for Laser-Based Manufacturing, School of Mechanical Engineering, Purdue University,

West Lafayette, Indiana 47907

Keywords:

Femtosecond laser ablation, aluminum, ablation rate, collisional absorption, collisionless absorption, early plasma.

Abstract

In this study, the ablation of aluminum by a near-infrared femtosecond laser pulse (800 nm, 100 fs) at different intensity is investigated by a two-dimensional hydrodynamic model. The ablation rates are compared between the cases in vacuum and in air over a wide range of laser power density. It has been reported before that at low ($<10^{13}$W/cm^2) and moderate laser intensity ($10^{13} – 10^{14}$W/cm^2), two different ablation regimes exist, and the ablation depth per pulse is dependent on the optical penetration depth and electron heat penetration depth, respectively. By considering both collisional and collisionless absorptions, the model in this study predicts the third ablation regime with a much higher ablation rate increase with respect to laser intensity in the high intensity range ($>10^{14}$W/cm^2) in vacuum, which shows good agreement with the experimental data. This phenomenon is attributed to the change of dominant absorption mechanism from collisional to collisionless absorption. For the case in air, the ablation depth

increases slowly with the laser intensity in the high intensity regime, and is much smaller than that in vacuum. It is revealed that this is due to the strong early plasma-laser interaction in air.

1. Introduction

The advantages of femtosecond laser radiation with a small heat-affected zone, low ablation threshold, and absence of plume plasma during the laser pulse promise its attractive applications in the realms of precise micromachining [1, 2], plasma state study [3, 4], and laser-induced breakdown spectroscopy [5, 6]. These promising applications make it necessary to understand the fundamental underlying physics, and a lot of investigations have been devoted to femtosecond laser pulse ablation of metals [7 – 21].

Experimental investigations [2, 8, 9] have indicated that the electron thermal diffusion can play an important role in the dissipation of absorbed photonic energy. Because of different heat dissipation mechanisms, ultrashort laser ablation of metals has been categorized by two different regimes at low ($< 5\times10^{12}$W/cm^2 for copper) and moderate ($5\times10^{12} – 1\times10^{14}$W/cm^2 for copper) laser intensity. As an example, the experimental measurement data for copper are shown in Fig. 1 [8]. The dependence of the ablation rate could be expressed by two different logarithmic functions [8, 9]:

$$L = \delta \ln\left(\frac{I}{I_{th}^{M}}\right) \tag{1}$$

$$L = \delta \ln\left(\frac{I}{I_{th}^{H}}\right) \tag{2}$$

where $!$ is the optical penetration depth, l is the electronic heat penetration depth, and I_{th}^{M}, I_{th}^{H} are the thresholds of ablation for the low and moderate laser intensity range, respectively. In the case of low-intensity ablation, the number density of hot electrons is so low that energy transfer occurs only within the area characterized by the optical penetration depth. However, in the case of moderate laser intensity, the density of hot electrons is high enough, and the contribution of the electron thermal diffusion to the dissipation of the absorbed energy causes a sudden increase in the ablation depth per pulse.

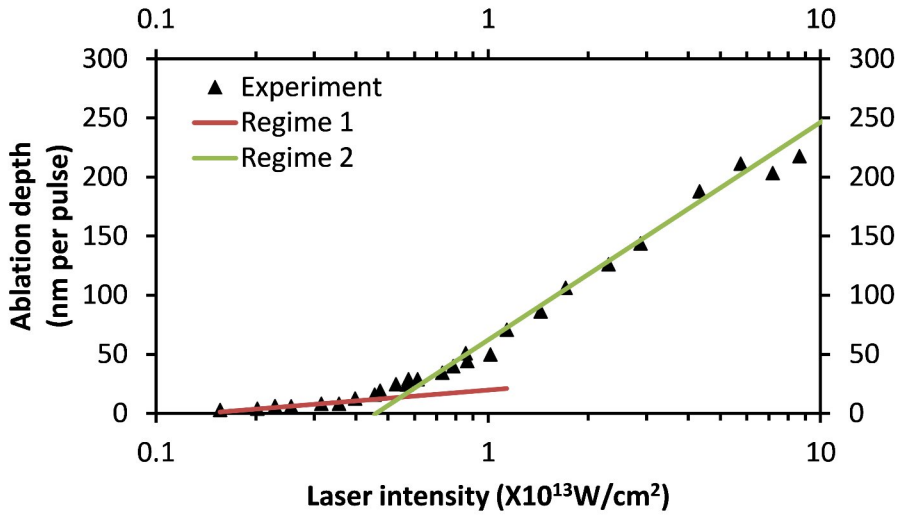

Fig. 1 Ablation depth per pulse for copper versus the incident laser intensity. Pulse duration: 150 fs, wavelength: 780 nm, target material: copper [8].

On the other hand, some experimental measurements [10 – 13] show that at high laser intensity (>1×10^{14}W/cm^2) in vacuum, there is a steep increase of ablation depth per pulse with respect to laser intensity, while ablation depth in air grows much slower. The change of ablation depth could possibly be affected by different ablation mechanisms, such as spallation [14, 15], phase explosion [16, 17], critical-point phase separation (CPPS) [13, 17], fragmentation [14],

and vaporization [14]. These mechanisms dominate in different laser intensity ranges, and may occur simultaneously, depending on the laser intensity. It has been reported that spallation usually dominates in the laser fluence range near the ablation threshold (2×10^{12} J/cm^2 for aluminum [15]), while the onsets of phase explosion, CPPS, and fragmentation were observed at the intensity of 5×10^{12} J/cm^2 [15], 5×10^{13} J/cm^2 [18], and 6×10^{12} J/cm^2 (2.8 times higher than the ablation threshold) [14] for aluminum, respectively. Vaporization should dominate at high laser intensity, but it only affects the topmost surface layer and do not contribute too much to the increase of ablation depth [14]. Therefore, the onset of ablation mechanisms mentioned above could not be responsible for the steep increase of the ablation rate in the high laser intensity range. It indicates that new mechanisms are involved, and a further investigation is necessary for a better understanding of relevant physics in this regime.

Different kinds of numerical models have been developed for ultrashort laser pulse ablation of metals, such as two-temperature models (TTM) [19-22], hydrodynamic models [13, 23, 24], and molecular dynamics models [14-17, 25]. Particularly, ablation rate and mechanisms of aluminum have been numerically studied in the low and moderate laser intensity range (below 10^{14} W/cm^2) [15, 18, 19, 20, 22, 23]. However, the ablation above 10^{14} W/cm^2 has been rarely discussed, and the effect of early stage plasma generation is seldom considered. In this work, a two dimensional computational model is presented for the prediction of the femtosecond laser ablation process in vacuum and in air. It comprises a two-dimensional (2D) axisymmetric hydrodynamic model and a two-temperature model, supplemented by an equation of state model to calculate the thermal and electrical properties of materials at different conditions [24]. By considering the collisionless absorptions and the ponderomotive force, the model is effective for

simulating relatively high-power ablation of metals, considering the effect of early plasma generation.

2. Theory and model

As shown in Fig. 2, the metal-ambient interface is located at z=0, and the symmetric axis is at r=0. Initially, the electron and lattice temperatures (T_e and T_i, respectively) are set to 300 K, and the velocities of electrons and ions are also set to zero ($\dot{v}_{e(i)} = 0$).

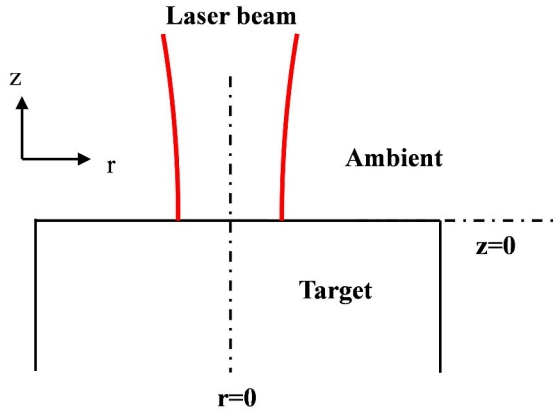

Fig. 2 Schematic diagram of the model setup.

2.1 Energy transfer inside the target

For ultrashort laser-material interactions, the electron and lattice temperatures are different before the thermodynamic equilibrium, and hence the energy transfer inside the target can be described by the well-known two-temperature model (TTM) [26, 27]:

$$C_e \frac{\partial T_e}{\partial t} = \frac{1}{r}\frac{\partial}{\partial r}\left[k_e r \frac{\partial T_e}{\partial r}\right] + \frac{\partial^2 T_e}{\partial z^2} - G(T_e - T_i) + S \tag{3}$$

$$C_i \frac{\partial T_i}{\partial t} = G(T_e - T_i) \tag{4}$$

where t is time, G is the electron-lattice coupling term [28], S is the laser absorption term, C_e, C_i, and k_e are the volumetric heat capacities of electrons and lattice, and electron thermal conductivity, respectively. The thermal and electrical properties of aluminum are calculated by the quotidian equation of state (QEOS) model [29].

2.2 Laser absorption

Both the collisional and collisionless absorptions are considered in the model. In metals, collisional absorption is considered to be dominant in most cases, due to the existence of sufficient free electrons. A free electron will gain laser beam energy by colliding with the bound electrons and lattice when wiggling in the oscillating laser field, which is known as inverse bremsstrahlung absorption, and the absorption rate of which can be calculated by [30]:

$$S = (1 - R)\alpha I_{surf}(r,z,t)\exp(-\alpha z) \quad (5)$$

where R, α, and I_{surf} denote the surface reflectivity, absorption coefficient, and laser intensity at the target surface, respectively. The optical properties of the target, such as the absorption coefficient and surface reflectivity are calculated based on Drude theory [31].

Collisionless absorption is the process where electrons directly absorb the laser beam energy without any collision process. When a laser beam is incident to an inhomogeneous plasma, the electric field's component along the plasma gradient will tend to drive the electrons to oscillate. The laser beam energy will be absorbed by electrons and get converted into their kinetic energy. At high laser intensity, because of the quick drop of the collisional absorption rate [23, 32], collisionless absorption becomes important and needs to be taken into account. The energy transfer process from the laser radiation to the matter should obey the Poynting's theorem [33]:

$$\frac{!u}{!t}!\ !\ !\dot{S}_p\ !\ !\ \dot{J}_e!\dot{E} \tag{6}$$

where $\dot{E}$ is the electric field intensity, $\dot{B}$ is the magnetic field density, $u = (\varepsilon_0\vec{E}^2 + \vec{B}^2/\mu_0)/2\,u\,!\ (!_0\dot{E}^2\ !\ \dot{B}^2\ /\ !_0)/2$ is the energy density of the laser electromagnetic field, and $\dot{S}_p\ !\ c^2!_0\dot{E}!\ \dot{B}$. The absorbed energy *S* is determined by the source term $!\ \dot{J}_e!\dot{E} - \vec{j}\cdot\vec{E}$. ($\dot{E}\,\vec{E}, \dot{B}\,\vec{B}$) are calculated from the Maxwell equations [24].

2.3 Electron dynamics and surface hot electron emission

The electron and ion dynamics inside the target is calculated by the drift-diffusion approach [34, 35]:

$$\frac{!n_e}{!t}!\ \frac{1}{e}!\ \ !\dot{J}_e\ !\ 0 \tag{7}$$

$$\frac{!n_i}{!t}!\ \frac{1}{e}!\ \ !\dot{J}_i\ !\ 0 \tag{8}$$

where e is the absolute value of electron charge, $n_e\,(n_i)$ and $\dot{J}_e\,(\dot{J}_i)$ are the number density and electric current density of electron (ion) [24].

There will be surface electron emission at the metal surface, and the total emission rate is the summation of thermal emission rate J_{th} and the n-photon photoelectric emission rate J_n given by [36]:

$$J_{th}\ !\ AT_{es}^2\exp\left[!\ !\ \frac{!}{k_BT_{es}}\right] \tag{9}$$

$$J_n = \alpha_n \left(\frac{e}{h\nu}\right)^n A T^2 (1-R)^n T_{es}^2 F\left(\frac{nh\nu - \phi}{k_B T_{es}}\right) \quad (10)$$

where T_{es} is the surface electron temperature, A is the theoretical Richardson coefficient equal to 120 A/cm^{2}K^2 [36], $\phi = 4.08eV$ [37] is the work function of aluminum, α_n is the n-photon photoelectric emission coefficient, for current case, $\alpha_2 = 0.85 \times 10^{-12} cm^2 s^{-2}$ [38], h denotes the Planck constant, ν is the photon frequency, and F represents the Fowler function.

2.4 Plasma dynamics

The electron and ion dynamics inside the plasma during the laser ablation can be simulated by the following hydrodynamic equations [24]:

$$\frac{\partial n_{e(i)}}{\partial t} + \nabla \cdot (n_{e(i)} \vec{v}_{e(i)}) = S_{e(i)} \quad (11)$$

$$\frac{\partial \vec{p}_{e(i)}}{\partial t} + \nabla \cdot (p_{e(i)} \vec{v}_{e(i)}) + \nabla (P_{e(i)}) = n_{e(i)} \vec{f}_{e(i)} \quad (12)$$

$$\frac{\partial \varepsilon_{e(i)}}{\partial t} + \nabla \cdot (\varepsilon_{e(i)} \vec{v}_{e(i)}) + \nabla \cdot (P_{e(i)} \vec{v}_{e(i)}) + \nabla \cdot \vec{q}_T = Q \quad (13)$$

where $\vec{p}_{e(i)}$, $P_{e(i)}$, and $\varepsilon_{e(i)}$ are the momentum, pressure, and total energy of electron (ion), respectively. Electrons in the plasma are treated as ideal gases in thermal equilibrium. $S_{e(i)}$ is the source term for electron (ion) generation in the bulk of the plasma, $\vec{f}_{e(i)}$ is the force term consisting of electric forces, collision forces and ponderomotive force, $\vec{q}_T$ is the thermal flux of

electrons (ions) by conduction, and Q is the energy term generated by collision, impact ionization, and recombination.

2.5 Laser power density distribution and air breakdown

The laser beam has a Gaussian profile and is focused by an external focal lens. The power density distribution is calculated as:

$$I(r,z) = 2I_0\left(\frac{w_0}{w(z)}\right)^2 \exp\left(\frac{-2r^2}{w^2(z)}\right) \tag{14}$$

where I_0 is the average power density over the focal spot (beam waist), w_0 is the beam waist size, and $w(z)$ is the radius of the beam spot at distance z given by:

$$w(z) = w_0\sqrt{1+\left(\frac{z}{z_R}\right)^2} \tag{15}$$

where $z_R = \frac{\pi w_0^2}{\lambda}$ is the Rayleigh range, λ is the laser wavelength. In this study, the laser beam has a wavelength of 800 nm and a beam waist of 25 μm. The focal length of the focal lens is 10 cm, and the focus spot is set on the target surface.

When the laser intensity is high enough, air molecules can be directly ionized by multi-photon ionization and air breakdown is initiated. The multi-photon ionization rate is calculated as [39, 40]:

$$R_{pi}(\lambda, x, t) = \sigma_k[I/h\nu]^k n_{ga} \tag{16}$$

where σ_k is the cross section for k-photon collision.

The ionized charged particles will assist and enhance further air breakdown by impact ionization, the rate of which is given by [39, 40]

$$R_{imp}(I,x,t) = \alpha_i(I)\, n_e(I) - 4\beta_i(I^2)\, U_I\, n_e(I^2)\, U_I \qquad (17)$$

where $\alpha_i(I) = 1.5(\frac{I}{U_I} - 1)^2$, U_I is the ionization energy of the atoms.

2.6 Numerical solution

All the governing equations are discretized by a finite volume method. A multigrid method and the convex essentially non-oscillatory (ENO) high order schemes [41] are adopted to solve the Maxwell equations and the hydrodynamic equations, respectively. At the metal-ambient interface, free boundary conditions are applied, and the electron and ion flux are determined by the hot electron emission rate and the ion dynamics inside the material, which are implemented as the boundary conditions for hydrodynamic eqns. (11)-(13) for the early plasma. Symmetric boundary conditions are adopted at the left boundary, while the fixed boundary conditions are applied at the upper, lower and right boundaries of the simulation domain, assuming they are not affected by the laser induced heat.

3. Results and discussions

Fig. 3 shows ablation depth per pulse as a function of laser intensity, for the cases both in air and in vacuum. The pulse duration is 100 fs, and the wavelength is 800 nm, and the target material is aluminum. Experimental data in literatures (in vauum: [42, 43], in air: [44]) are shown to compare with the simulation results. The detailed parameters used in the simulation and the experiments are summarized in Table 1. The pulse duration in [44] is 120 fs, which is

slightly different from the value used in the simulation (100 fs). However, since the ablation depth is not sensitive to the pulse duration up to 1 ps [12], it is valid to compare these results together. Besides, the focal lens in [43] has a long focal length (25 cm) compared with the others (10 cm). It has been reported that the focal length could affect the absorption of laser beam energy by air breakdown in air [45]. However, this becomes the minor effect in vacuum since there is no air breakdown. In the model, the ablation depth is calculated based on the assumption of critical-point phase separation [13], where the material is first heated to a very high temperature in a solid state density, and then cools down to reach the critical point, followed by a phase separation inducing the material removal process. The ablation depth is determined by the location where the local temperature exceeds the separation temperature, which is the minimum temperature required for the material to be ablated [13]. The simulation results show very good agreement with the experimental data. In the low intensity regime ($<10^{13}$W/cm^2), the ablation depths are similar between in air and in vacuum. At moderate intensity (10^{13}W/cm^2 ~ 10^{14}W/cm^2), the ablation depths in vacuum become slightly higher. When the laser intensity further increases, there is a steep increase of the ablation depth in vacuum, and a third ablation regime forms. On the contrary, the ablation depth in air increases slowly with the laser intensity, and tends to saturate as the laser intensity rises to a very high value. The ablation depth in vacuum is 7 times larger than that in air at the laser intensity of 10^{15}W/cm^2.

Data	Pulse duration (fs)	Wavelength (nm)	Focal length (cm)
Simulation in this study	100	800	10
Experiment in [42] (vacuum)	100	800	10
Experiment in [43] (vacuum)	100	800	25
Experiment in [44] (in air)	120	800	10

Table 1 Laser and focal lens parameters in the simulation and literatures.

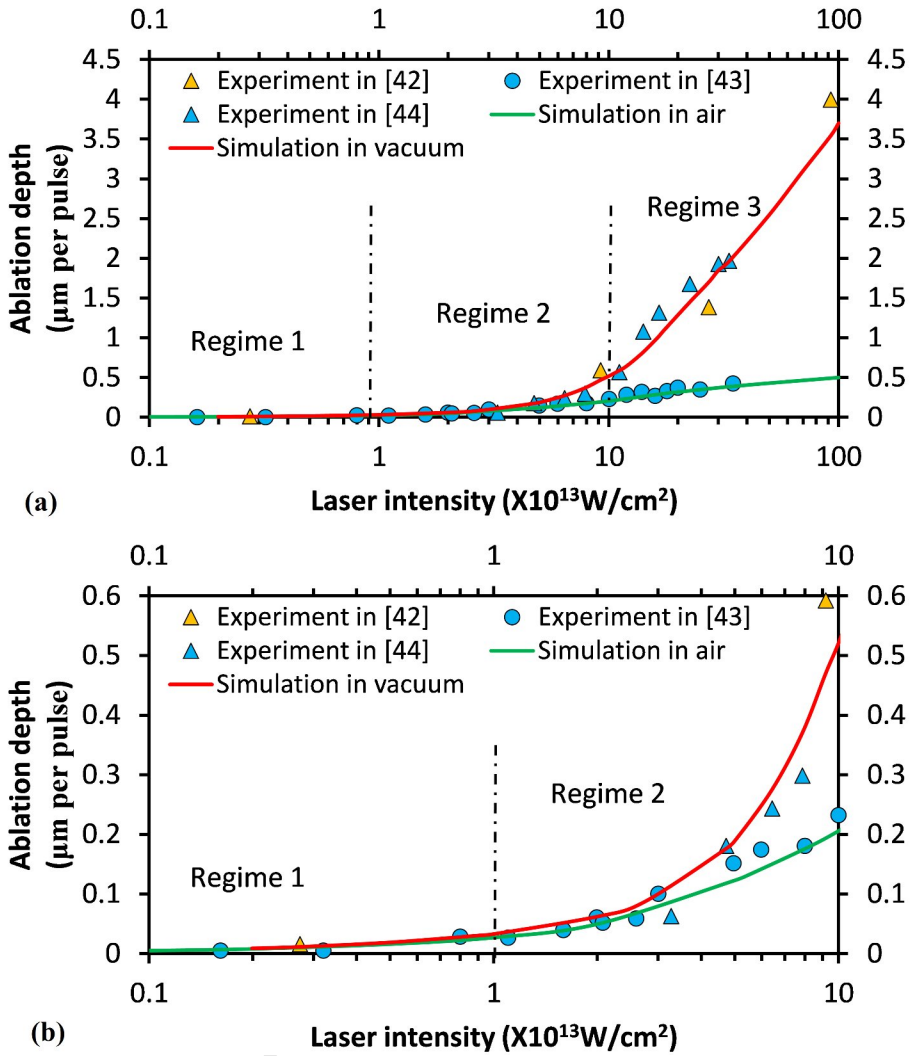

Fig. 3 Ablation depth per pulse as the function of intensity (a) from low to high laser intensity, and (b) zoom in the low and moderate laser intensity range. Pulse duration of 100 fs, wavelength of 800 nm, target material: aluminum. The experimental data in vacuum is from [42, 43], and the data in air is from [44].

It has been proved that with increased laser intensity ($> 10^{15}$W/cm^2), the collisions between electrons and ions become less effective, and the collisional absorption model alone fails to explain the level of absorbed laser beam energy experimentally observed [46-48]. Meanwhile,

the collisionless absorption rate increases with laser intensity, and it is possible to become the dominate absorption process in the high intensity regime. Fig. 4 represents the calculated variation of absorptivity from low to high laser intensity. The absorptivities of the collisional absorption, the collisionless absorption, and the total absorption are compared, and validated by the experimental measurements derived from the reflectivity data in [49]. Below moderate laser intensity ($<10^{14}$W/cm^2), the total absorptivity increases with the laser intensity, and is mainly determined by the collisional absorption. The collisionless absorption is negligible in this range. However, as the laser intensity further increases, the collisional absorption rate decreases fast because of the drop of effective collision frequency at high plasma temperature [23]. In the mean time, the collisionless absorption rate rises with the increase of the electromagnetic field induced by the laser pulse. It gradually becomes important and dominant in the absorption process. It can be seen that at high laser intensity, the collisional absorption alone significantly underestimates the total absorptivity. At the laser intensity of 10^{15}W/cm^2, the absorptivity is underestimated by 80% by the collisional absorption. This observation agrees with the conclusions in [46-48] that the collisionless absorption will become the dominant absorption mechanism in the high laser intensity range. By considering the collisionless absorption, the simulation results show a good agreement with the experimental data in a wide range of laser intensity. The switch of the dominant absorption mechanism may have a significant effect on the absorption rate, heat diffusion depth and the ablation depth. Based on the analysis as shown in Fig. 4, at high laser intensity, most of the laser beam energy is absorbed by the collisionless absorption, and the total absorptivity increases quickly accordingly. The absorbed laser beam energy can then be dissipated deeper into the target by the electron thermal diffusion, consequently leading to a sudden rise of ablation depth. Therefore, the sudden increase of the ablation depth at high laser

intensity can be attributed to the involvement of the collisionless absorption and the resultant deeper penetration depth.

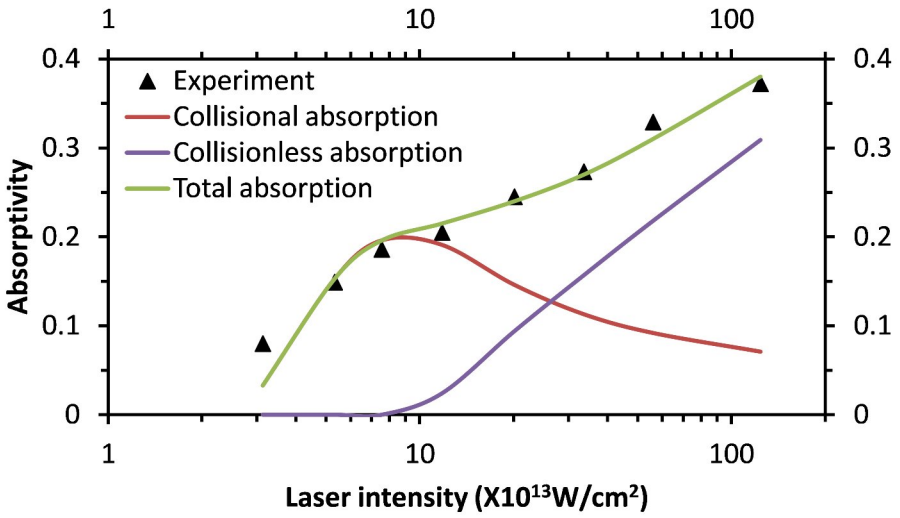

Fig. 4 Absorptivity of the target at different laser intensity. Pulse duration: 100 fs, wavelength: 800 nm, target material: aluminum. Experimental data is from [49].

In the high intensity regime, the ablation depth in air increases slowly with laser intensity, and the ablation rate is much lower than that in vacuum. The dissimilarity between the ablation depth trends in air and in vacuum is attributed to air breakdown and early plasma generation in air. When the laser intensity is high enough, the laser induced air breakdown will occur by multi-photon ionization. Besides, a strong early plasma will be formed above the target within the pulse duration by surface hot electron emission and the resultant air ionization [25]. This early plasma and air breakdown can both absorb the incident laser beam energy and decrease the energy deposited into the target, thus decreasing the ablation rate significantly. Fig. 5 shows the portion of the laser beam energy absorbed by the early plasma and air breakdown as a function of laser intensity. The external focal lens has a focal length of 10 cm. It can be seen that the early plasma absorption starts from 10^{14} W/cm^2, while the threshold of air breakdown is around 3X10^{13}

W/cm^2. Besides, air breakdown is the dominant absorption process, especially in the low laser intensity range. The laser beam energy consumed by air breakdown is over 2 times higher than the loss due to the early plasma absorption.

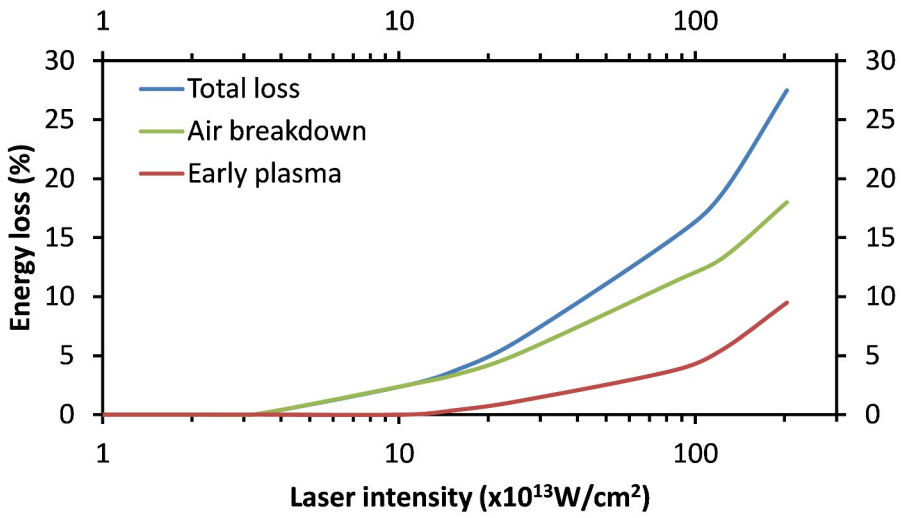

Fig. 5 Laser beam energy loss due to early plasma absorption. Pulse duration:100 fs, wavelength: 800 nm, target material: aluminum.

Fig. 6 compares the energy loss of the incident laser beam in air and in vacuum at different laser intensity with the same laser and lens parameters as the cases above. For the ablation in vacuum, there is no laser induced air breakdown, and the ejected energetic electrons will diffuse freely into the vacuum without any ionization process. The absorption by the hot electrons is the only absorption mechanism of the incident laser beam energy, and the absorption rate is very low because the number density of the electrons in vacuum is small and the collision frequency is low. Therefore, at the same laser intensity, the energy loss of the incident laser beam in vacuum is much lower and negligible, compared with that in air. Accordingly, the laser beam energy deposited into the target material will be much lower in air, leading to a lower ablation depth at

high laser intensity. That explains why the ablation rate in air is much lower than that in vacuum, and in the high fluence range, the ablation rate tends to saturate.

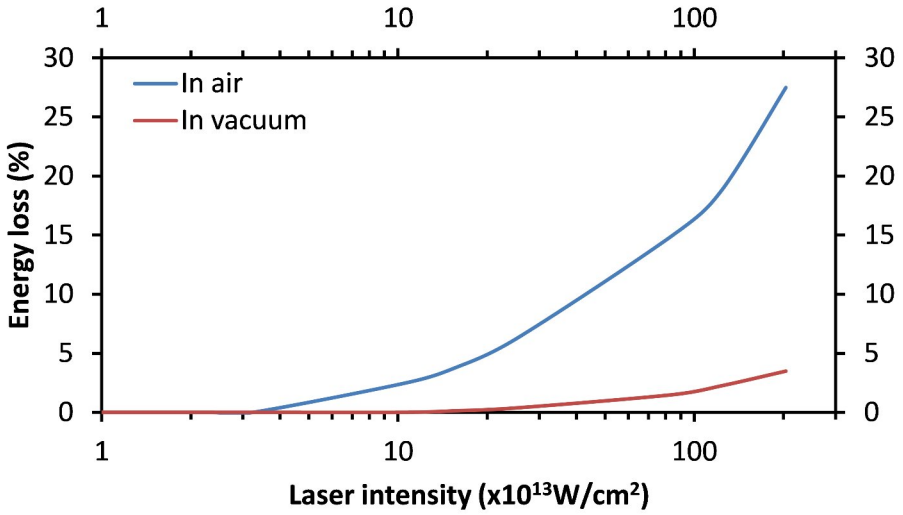

Fig. 6 The incident laser beam energy loss in air and in vacuum. Pulse duration:100 fs, wavelength: 800 nm, target material: aluminum.

4. Conclusions

Femtosecond laser ablation of aluminum from low to high laser intensity has been investigated by a 2D axisymmetric hydrodynamic model. The ablations in air and in vacuum were compared, and the underlying physics mechanisms were analyzed. It is revealed that at low and moderate laser intensity (below 10^{14}W/cm^2), the ablation depths per pulse in air an in vacuum are similar. In the high laser intensity regime (above 10^{14}W/cm^2), there is a steep rise of the ablation depth in vacuum, while the ablation rate in air increases slowly with laser intensity. At the laser intensity of 10^{15}W/cm^2, the ablation depth in vacuum is 7 times higher than that in air. The steep change of the ablation depth in vacuum is due to the involvement of the collisionless absorption at high laser intensity. At low and moderate laser intensity, the

collisional absorption is the dominant mechanism and the total absorptivity increases with laser intensity. At high laser intensity, the collisional absorption is reduced and the corresponding absorption rate drops quickly, while the collisionless absorption increases with laser intensity and becomes the dominant absorption mechanism. At the laser intensity of 10^{15}W/cm^2, the absorption by collisionless absorption is 4 times higher than that of collisional absorption. The low ablation rate at high laser intensity in air is because of strong early plasma-laser interaction. The early plasma absorption occurs at the laser intensity of 10^{14}W/cm^2, and air breakdown initiates from $3X10^{13}$ W/cm^2. It is shown in this study that the air breakdown is the dominant absorption mechanism, compared with the early plasma absorption, which consumes over 70% of the total energy loss of the incident laser beam. Because of the air breakdown and the early plasma generation in air, the absorption in air is much stronger than that in vacuum (9 times higher at the laser intensity of 10^{15}W/cm^2).

Acknowledgement:

The authors wish to gratefully acknowledge the financial support provided for this study by the National Science Foundation (Grant No: 0853890-CBET, 0917936-IIP).

References:

[1] C. Momma, S. Nolte, B.N. Chichkov, F.V. Alvensleben, A. Tünnermann, Precise laser ablation with ultrashort pulses, Appl. Surf. Sci. 109/110 (1997) 15-19.

[2] K. Furusawa, K. Takahashi, H. Kumagai, K. Midorikawa, M. Obara, Ablation characteristics of Au, Ag, and Cu metals using a femtosecond Ti:sapphire laser, Appl. Phys. A: Mater. Sci. Process 69S (1999) 359-366.

[3] H.M. Milchberg, R.R. Freeman, S.C. Davey, R.M. More, Resistivity of a simple metal from room temperature to 10^6 K, Phys. Rev. Lett. 61 (1988) 2364-2367.

[4] S.S. Mao, X. Mao, R. Greif, R. E. Russo, Initiation of an early-stage plasma during picosecond laser ablation of solids, Appl. Phys. Lett. 77 (2000) 2464-2466.

[5] V. Margetic, A. Pakulev, A. Stockhaus, M. Bolshov, K. Niemax, R. Hergenröder, A comparison of nanosecond and femtosecond laser-induced plasma spectroscopy of brass samples, Spectrochim. Acta Part B 55 (2000) 1771-1785.

[6] K. Stelmaszczyk, P. Rohwetter, G. Méjean, J. Yu, E. Salmon, J. Kasparian, R. Ackermann, J. Wolf, L. Wöste, Long-distance remote laser-induced breakdown spectroscopy using filamentation in air, Appl. Phys. Lett. 85 (18) (2004) 3977-3979.

[7] B. Oh, D. Kim, J. Kim, J. Lee, Femtosecond laser ablation of metals and crater formation by phase explosion in the high-fluence regime, J. Phys.: Conf. Ser. 59 (2007) 567-570.

[8] S. Nolte, C. Momma, H. Jacobs, A. Tünnermann, Ablation of metals by ultrashort laser pulses, J. Opt. Soc. Am. B 14 (10) (1997) 2716-2722.

[9] Y.V. Afanasiev, N.N. Demchenko, V.A. Isakov, I.N. Zavestovskaia, B.N. Chichkov, Threshold characteristics of short and ultrashort laser pulse ablation of metals, Proc. of SPIE 4760 (2002) 424-431.

[10] P.A. Atanasov, N.N. Nedialkov, Influence of the processing parameters on the ultrashort laser ablation of metals, Proc. of SPIE 6346 (2007) 63462Y.

[11] N.N. Nedialkov, S.E. Imamova, P.A. Atanasov, G. Heusel, D. Breitling, A. Ruf, H. Hugel, F. Dausinger, P. Berger, Laser ablation of iron by ultrashort laser pulses, Thin Solid Films 453 –454 (2004) 496-500.

[12] A.M. Komashko, M.D. Feit, A.M. Rubenchik, M.D. Perry, P.S. Banks, Simulation of material removal efficiency with ultrashort laser pulses, Appl. Phys. A 69 (1) (1999) S95-S98.

[13] F. Vidal, T.W. Johnston, S. Laville, O. Barthélemy, M. Chaker, B. Le Drogoff, J. Margot, M. Sabsabi, Critical-point phase separation in laser ablation of conductors, Phys. Rev. Lett. 86 (12) (2001) 2573–2576.

[14] D. Perez, L.J. Lewis, Molecular-dynamics study of ablation of solids under femtosecond laser pulses, Phys. Rev. B 67 (2003) 184102.

[15] N.N. Nedialkov, S.E. Imamova, P.A. Atanasov, P. Berger, F. Dausinger, Mechanism of ultrashort laser ablation of metals: molecular dynamics simulation, Appl. Surf. Sci. 247 (2005) 243-248.

[16] P. Lorazo, L.J. Lewis, M. Meunier, Short-pulse laser ablation of solids: from phase explosion to fragmentation, Phys. Rev. Lett. 91 (2003) 225502.

[17] W. Hu, Y. Shin, G. King, Energy transport analysis in ultrashort pulse laser ablation through combined molecular dynamics and Monte Carlo simulation, Phys. Rev. B 82 (2010) 094111.

[18] M.E. Povarnitsyn, T.E. Itina, M. Sentis, K.V. Khishchenko, P.R. Levashov, Material decomposition mechanisms in femtosecond laser interactions with metals, Phys. Rev. B 75 (2007) 235414.

[19] B.H. Christensen, K. Vestentoft, P. Balling, Short-pulse ablation rates and the two-temperature model, Appl. Surf. Sci. 253 (2007) 6347–6352.

[20] B. Wu, Y.C. Shin, A simple model for high fluence ultra-short pulsed laser metal ablation, Appl. Surf. Sci. 253 (2007) 4079-4084.

[21] B. Wu, Y.C. Shin, A simplified predictive model for high-fluence ultra-short pulsed laser ablation of semiconductors and dielectrics, Appl. Surf. Sci. 255 (2009) 4996–5002.

[22] Q. Li, H. Lao, J. Lin, Y. Chen, X. Chen, Study of femtosecond ablation on aluminum film with 3D two-temperature model and experimental verifications, Appl. Phys. A 105 (2011) 125–129.

[23] K. Eidmann, J. Meyer-ter-Vehn, T. Schlegel, Hydrodynamic simulation of subpicosecond laser interaction with solid-density matter, Phys. Rev. B 62 (1) (2000) 1202-1214.

[24] X. Zhao, Y.C. Shin, A two-dimensional comprehensive hydrodynamic model for femtosecond laser pulse interaction with metals, J. Phys. D: Appl. Phys. 45 (2012) 105201.

[25] W. Hu, Y. Shin, G. King, Early-stage plasma dynamics with air ionization during ultrashort laser ablation of metal, Phys. Plasmas 18 (2011) 093302.

[26] S.I. Anisimov, B.L. Kapeliovich, T.L. Perel'man, Electron emission from metal surfaces exposed to ultra short laser pulses, Sov. Phys. JETP 39 (1974) 375-377.

[27] T.Q. Qiu, C.L. Tien, Heat Transfer Mechanisms During Short-Pulse Laser Heating of Metals, J. Heat Transfer 115 (1993) 835–841.

[28] S. Laville, F. Vidal, T.W. Johnston, O. Barthelemy, M. Chaker, B.L. Drogoff, J. Margot, M. Sabsabi, Fluid modeling of the laser ablation depth as a function of the pulse duration for conductors, Phys. Rev. E 66 (2002) 066415.

[29] R.M. More, K.H. Warren, D.A. Young, G.B. Zimmerman, A new quotidian equation of state (QEOS) for hot dense matter, Phys. Fluids 31 (1988) 3059-3078.

[30] C. Schäfer, H.M. Urbassek, L.V. Zhigilei, Metal ablation by picosecond laser pulses: a hybrid simulation, Phys. Rev. B 66 (2002) 115404.

[31] F.L. Pedrotti, L.S. Pedrotti, Introduction to Optics, Englewood Cliffs/Prentice Hall, Upper Saddle River, NJ, 1993.

[32] D.F. Price, R.M. More, R.S. Walling, G.Guethlein, R.L. Shepherd, R.E. Stewart, W.E. White, Absorption of ultrashort laser pulses by solid targets heated rapidly to temperatures 1-1000 eV, Phys. Rev. Lett. 75 (2) (1995) 252-255.

[33] M. Born, E. Wolf, *Principles of Optics*, 4th edition, Pergamon Press, Oxford, 1970.

[34] N.M. Bulgakova, R. Stoian, A. Rosenfeld, I.V. Hertel, E.E.B. Campbell, Electronic transport and consequences for material removal in ultrafast pulsed laser ablation of materials, Phys. Rev. B 69 (2004) 054102.

[35] N.M. Bulgakova, R. Stoian, A. Rosenfeld, I.V. Hertel, W. Marine, E.E.B. Campbell, A general continuum approach to describe fast electronic transport in pulsed laser irradiated materials: The problem of Coulomb explosion, Appl. Phys. A 81 (2005) 345-356.

[36] J.H. Bechtel, W. Lee Smith, N. Bloembergen, Two-photon photoemission from metals induced by picosecond laser pulses, Phys. Rev. B 15 (1977) 4557- 4563.

[37] P.A. Tipler, R.A. Llewellyn, Modern Physics, 3rd Ed., W.H. Freeman, New York, 1999.

[38] P. Martin, R. Trainham, P. Agostini, G. Petite, Electron and ion emission in high-intensity laser irradiation of aluminum, Phys. Rev. B 45 (1) (1992) 69-77.

[39] B.C. Stuart, M.D. Feit, S. Herman, A.M. Rubenchik, B.W. Shore, M.D. Perry, Nanosecond-to-femtosecond laser-induced breakdown in dielectrics, Phys. Rev. B 53 (1996) 1749-1761.

[40] X. Lin, J. Yanga, Y. Suna, S. Jianga, Ultra-short laser ablation of dielectrics: Theoretical analysis of threshold damage fluence and ablation depth, Appl. Surf. Sci. 256 (2009) 130-135.

[41] X. Liu, S. Osher, Convex ENO High Order Multi-dimensional Schemes without Field by Field Decomposition or Staggered Grids, J. Comput. Phys. 142 (2) (1998) 304–330.

[42] N.N. Nedialkov, P.A. Atanasov, D. Breitling, G. Heusel, F. Dausinger, Ablation of metals by ultrashort laser pulses, Proc. of SPIE 5830 (2005) 80-84.

[43] J-M. Savolainen, M.S. Christensen, P. Balling, Material swelling as the first step in the ablation of metals by ultrashort laser pulses, Phys. Rev. B 84 (2011) 193410.

[44] R. Le Harzic, D. Breitling, M. Weikert, S. Sommer, C. Föhl, F. Dausinger, S. Valette, C. Donnet, E. Audouard, Ablation comparison with low and high energy densities for Cu and Al with ultra-short laser pulses, Appl. Phys. A 80 (2005) 1589–1593.

[45] W. Hu, Y.C. Shin, G.B. King, Effect of air breakdown with a focusing lens on ultrashort laser ablation, Appl. Phys. Lett. 99 (2011) 234104.

[46] C.T. Hansen, S.C. Wilks, P.E. Young, Spectral Evidence for Collisionless Absorption in Subpicosecond Laser-Solid Interactions, Phys. Rev. Lett. 83 (24) (1999) 5019-5022.

[47] M.K. Grimes, A.R. Rundquist, Y.-S. Lee, M.C. Downer, Experimental identification of "vacuum heating" at femtosecond-laser-irradiated metal surfaces, Phys. Rev. Lett. 82 (20) (1999) 4010-4013.

[48] L.M. Chen, J. Zhang, Q.L. Dong, H. Teng, T.J. Liang, L.Z. Zhao, Z.Y. Wei, Hot electron generation via vacuum heating process in femtosecond laser-solid interactions, Phys. Plasmas 8 (6) (2001) 2925-2929.

[49] P.S. Komarov, S.I. Ashitkov, A.V. Ovchinnikov, D.S. Sitnikov, M.E. Veysman, P.R. Levashov, M.E. Povarnitsyn, M.B. Agranat, N.E. Andreev, K.V. Khishchenko, V.E. Fortov, Experimental and theoretical study of Al plasma under femtosecond laser pulses, J. Phys. A: Math. Theor. 42 (2009) 214057.

Highlights:

- Femtosecond ablation of aluminum at high laser intensity is studied.
- There is a steep increase of the ablation depth in vacuum at high intensity.
- The collisionless absorption becomes dominating in this range.
- Air breakdown and early plasma absorption leads to lower ablation depth in air.